metals

MDPI

Article

Co_2CrAl Heuslerene: Mechanical, Thermodynamic and Electronic Properties

Arash Boochani [1,2,*], Moein Asshabi [3], Jabbar Khodadadi [3], Elmira Sartipi [2], Morteza Jamal [4], Jamshid Sabbagzadeh [2], Masoud Shahrokhi [5], Malieheh Amiri [1], Arash Yari [1], Shahram Solaymani [2,*], Amir hossein Sari [2] and Saeid Jalali-Asadabadi [6]

1 Department of Physics, Kermanshah Branch, Islamic Azad University, Kermanshah 6718997551, Iran
2 Quantum Technologies Research Center (QTRC), Science and Research Branch, Islamic Azad University, Tehran 1343864331, Iran
3 Department of Physics, Razi University, Kermanshah 94Q5+6G3, Iran
4 Young Researchers and Elite Club, Shahr-e-Qods, Islamic Azad University, Shahr-e-Qods M4Q7+FCH, Iran
5 Young Researchers and Elite Club, Kermanshah Branch, Islamic Azad University, Kermanshah 6718997551, Iran
6 Department of Physics, Faculty of Physics, University of Isfahan (UI), Hezar Jerib Avenue, Isfahan 8174673441, Iran
* Correspondence: arash_bch@yahoo.com (A.B.); shahram22s2000@yahoo.com or shahram.solaymani@ipm.ir (S.S.)

Abstract: This work investigates the ground state's stability of the bulk and three Heuslerene Co_2CrAl compounds, named as α, β, and γ phases, by density functional theory (DFT) with the generalized gradient approximation (GGA), GGA+U, and GGA+U+mBJ approximations. The results demonstrate the ground state stability of all mentioned cases since they pass the thermodynamic, elastic, and phonon stability tests. All three structures are more stable in the ferromagnetic phase than the antiferromagnetic phase. In the β phase, Young's and Shear's moduli were 73.97 GPa and 24.83 GPa, respectively. The thermodynamic diagram has shown existence of the accessible region, which indicates the possibility of making this structure. For all three structures, the phonon branches in the symmetry paths are positive, which represent the complete dynamic stability of these compositions in the presence of mechanical stresses and thermal vibrations. According to the electronic calculations, the bulk phase of Co_2CrAl is a half-metal with $3\mu_B$ magnetic moment and 100% spin polarization at the Fermi level. Furthermore, all imposed approximations approve that α and γ Heuslerenes are metal for both spin directions, while the GGA+U+mBJ approximation indicates that β phase is a ferromagnetic half-metal of $1\mu_B$ magnetic moment. Based on the electron density diagrams, the highest (lowest) amount of electron density is created on the α (β) phase surface.

Keywords: DFT; Co_2CrAl Heuslerene; elastic stability; dynamic stability; phase diagram; electronic structure

check for updates

Citation: Boochani, A.; Asshabi, M.; Khodadadi, J.; Sartipi, E.; Jamal, M.; Sabbagzadeh, J.; Shahrokhi, M.; Amiri, M.; Yari, A.; Solaymani, S.; et al. Co_2CrAl Heuslerene: Mechanical, Thermodynamic and Electronic Properties. *Metals* **2023**, *13*, 582. https://doi.org/10.3390/met13030582

Academic Editor: Carlos Capdevila-Montes

Received: 18 January 2023
Revised: 16 February 2023
Accepted: 7 March 2023
Published: 13 March 2023

Copyright: © 2023 by the authors. Licensee MDPI, Basel, Switzerland. This article is an open access article distributed under the terms and conditions of the Creative Commons Attribution (CC BY) license (https://creativecommons.org/licenses/by/4.0/).

1. Introduction

The unique properties of spin devices based on Heusler alloys motivated scientists to develop their fundamental knowledge about applying these materials for industrial and research applications. Ferromagnetic materials with Heusler compounds have significant applications in various modern technologies like data storage, sensors, and energy conversion [1,2]. Simplicity in manufacturing, high mechanical resistance, low-cast and availability of materials as well as high Curie temperature of Heusler compounds have made them good candidates for using in spintronics, opto-electronic, giant magneto resistance (GMR), tunneling magneto resistance (TMR), magnetic thermoelectric applications, magneto-optic devices [3–9].

The synthesis of Co-based Heusler compounds began in 1970s [10]. Kübler et al. [11] found the disappearance of the minority spin density at the Fermi level of Co_2MnSn

and Co_2MnAl, resulted from the specific transport of the majority spin density towards meeting the Fermi level. Meanwhile, de Groot et al. [12] introduced half-metals (HM) ferromagnets (HMFMs) with 100% spin polarization at Fermi level, as ideal candidates for spintronic devices with spin injection [13]. Band structure (BS) of Heusler compounds has the important role in describing their magnetic characterization and prediction of HMFMs. The first attempts to calculate the BS of some Co-based Heusler compounds (Co_2MnSn, Co_2TiSi, and Co_2TiAl) did not show HM ferromagnetism since the basis of calculations were spherical potentials. Moreover, the simple form of exchange-correlation potential was approximated by local spin density approximation (LSDA) [14–18]. Ishida et al. revealed the first signs of HM ferromagnetism in Co-based Heusler compounds for Ru_2MnC and Co_2MnC (C = Si, Al, Sb, and Sn) [19,20]. Mohn et al. [21] could only find the magnetic ground state of Co_2TiC (C = Sn and Al) by full symmetry potentials, not the HM state. Also, Galanakis et al. [22] reported HM behavior in various A_2BC compounds which was in good agreement with those found by Picozi. et al. for the Mn-based compounds. They used the GGA because, despite the pure LSDA function, the GGA technique considers the gradients of density [23]. Verifying the HM state of Co_2FeAl is not possible by spherical potentials or GGA approximation and for the complete series of $Co_2Cr_{1-xx}Fe_xAl$, the HM ferromagnetic ground state can be found when both GGA approximation and full symmetry potentials are applied [24,25].

The ferromagnetic properties with the significant magnetic moment and high Curie temperature were observed in the majority spin of Co-based full Heusler compounds with cubic L_{21} structure [26]. The Curie temperature and magnetic moment of Co_2MnSi are 985 K and 4.96 μB, respectively. Furthermore, many of them were predicted to be half-metal and hence, are of particular interest in spintronic devices [27–30]. Recently, the electronic BS and magnetic properties of full Heusler compounds have been investigated on a large scale, both theoretically and experimentally [26–28]. For instance, the total magnetic moments in these compounds followed the Slater-Pauling-type behavior and were explained by their electronic structures [23]. Also, the high Curie temperatures of Co-based Heulser compounds were calculated by ab initio calculations related to the electronic structures [27].

The popularity of two-dimensional (2D) materials with few atoms thickness started in 2004 by discovery of graphene. These materials are considered as promising candidates for the next generation of optoelectronics and electronics devices, because of their mechanical, thermal, and electrical properties [28,31,32]. Graphene is a single layer of sp^2-bonded carbon atoms with high carrier mobility [33] which is almost chemically inert [34]. Its mechanical flexibility [35] makes it to be applied in flexible electronic and ultrathin 2D devices. Therefore, graphene has a wide variety of applications in transistors as well as chemical and strain sensors [36,37]. For group-IV 2D materials like silicone, graphene, stanene, and germanene, the zero band gap can be opened by the adsorption of special species or vertical electric field. However, their application in transistors is restricted at room temperature because in general, the value of opened band gap is smaller than 0.4 eV [38,39]. Recently, materials such as nitrogenene [40], black phosphorene (BP) [41], arsenene [42], and antimonene [43] in group-V 2D have attracted great attention. The direct band gap of monolayer and few-layer BP is almost 0.59–1.51 eV [44] and its unique electronic properties like ON/OFF current ratio and high carriers mobility (∼1000 cm^2/Vs) indicate its necessity in electronic and optoelectronic applications [45–47]. The discovery of semiconductors and insulators has expanded 2D materials and graphene over the past few years [48,49]. Using the 2D structures of the direct band gap semiconductors in transition metal dichalcogenides (TMDs) like monolayer WS_2 and MoS_2 have significantly improved optoelectronics devices [50,51]. However, further improvements require continuous investigations of new 2D materials. Current methods for creating 2D monolayers cannot be used in bulk-layered materials since their access to crystals has not been explored yet [52].

The high compactness with mechanical stability of the FCC thin films and 2D hexagonal structures along their [111] crystallographic direction make them a suitable candidate for electronic devices. In our last works, the graphene-like monolayers of Ti_2VGe and Co_2CrAl

Heusler compounds were made along the [111] direction and named Heuslerenes [53,54]. According to the DFT-based calculations, the two mentioned Heuslerenes were stable from the static and dynamic viewpoins. In addition, electronic calculations by GGA and mBJ approximations revealed them to be half-metals. The main goal of the present work is to expand the idea of Heuslerenes based on Co_2CrAl and dealing with their expected properties in some details.

Considering the half-filled *d* orbitals of two Co and Cr atoms in the Co_2CrAl compound, we expect to see a half-metallic behavior by cutting the Co_2CrAl FCC structure and creating 2D compounds named as Co_2CrAl Heuslerenes. Therefore, for feasibility of making them, at first step, we calculate the formation energy and show that it is possible to form theses combinations. Then we look for the ground state point to show the existence of mechanical stability in the static mode. In the following, stability of these structures under stress and strain is checked by evaluating their elastic coefficients. At the next step, the mechanical stability will be evaluated from the vibration point of view by means of phonon dispersion diagrams. Furthermore, to complete the possibility of making these compounds in reality, thermodynamic phase diagrams are obtained, the electronic properties of these compounds in the ferromagnetic phase are discussed by drawing the density of states (DOS), BS and electron density diagrams.

2. Computational Methods

The electronic structure, thermodynamic phase diagram and mechanical stability of Co_2CrAl in the bulk and Heuslerene phases were studied by density functional theory (DFT) and full potential linearized augmented plane waves (FP-LAPW) method [55] such as our previous research [56]. The exchange-correlation potential in the Wien2K [57] code were calculated by generalized gradient approximation (GGA) [58], GGA+U [59,60], and GGA+U+mBJ [61,62] approximations. Our calculations considered by spin polarization mode and Hubbard potential (U) of the Co and Cr atoms were optimized as 0.235 Ry and 0.0, respectively. The optimized $R_{mt}K_{max}$ parameter is 8 and the Brillouin zone *KPoint* for the bulk and Heuslerens are $17 \times 17 \times 17$ and $19 \times 19 \times 5$, respectively. The muffin tin radius of Co and Cr atoms is 2.15 a.u. and for Al is 2.00 a.u. Elastic constants of the bulk and Heuslerene crystals were proposed by Jamal [56,63,64] considering the Hubbard U parameter (GGA+U) in the Wien2K framework. In order to show the crystal dynamical stability, phonon dispersions have been extracted from the Quantum Espresso package [65,66]. For increasing the accuracy of phonon calculations, and other electronic results the atomic forces were relaxed up to the best optimization of 10^{-6} (a.u./dyn) and the optimized *k*-point and *q*-point meshes for phonon calculations were selected as $24 \times 24 \times 3$ and $10 \times 10 \times 2$, respectively. To calculate the mechanical, thermodynamic phase diagram, and electronic properties, we used from the 40 core super computer in six month.

3. Results and Discussion

3.1. Stability of the Bulk and 2D Sheets of Co_2CrAl

3.1.1. Structural Stability

Co_2CrAl is a Co-based full-Heusler compound crystallized in F.C.C. structure with space group of $Fm\bar{3}m$. As mentioned above, the layers cut along its [111] crystallographic direction must be hexagonal, dense enough, and stable. Thus, considering the atomic termination of the slices, we have produced three ultrathin films of about 8 Bohr thick, named as α, β and γ phases (see Figure 1) with *p3m1* space group. It is important to note that the stoichiometry of each product is different from the main source, as Co_2CrAl_2, Co_2Cr_2Al, and Co_3CrAl for the α, β, and γ shapes, respectively. We will see that this extra atom in each monolayer plays a positive role in its stability.

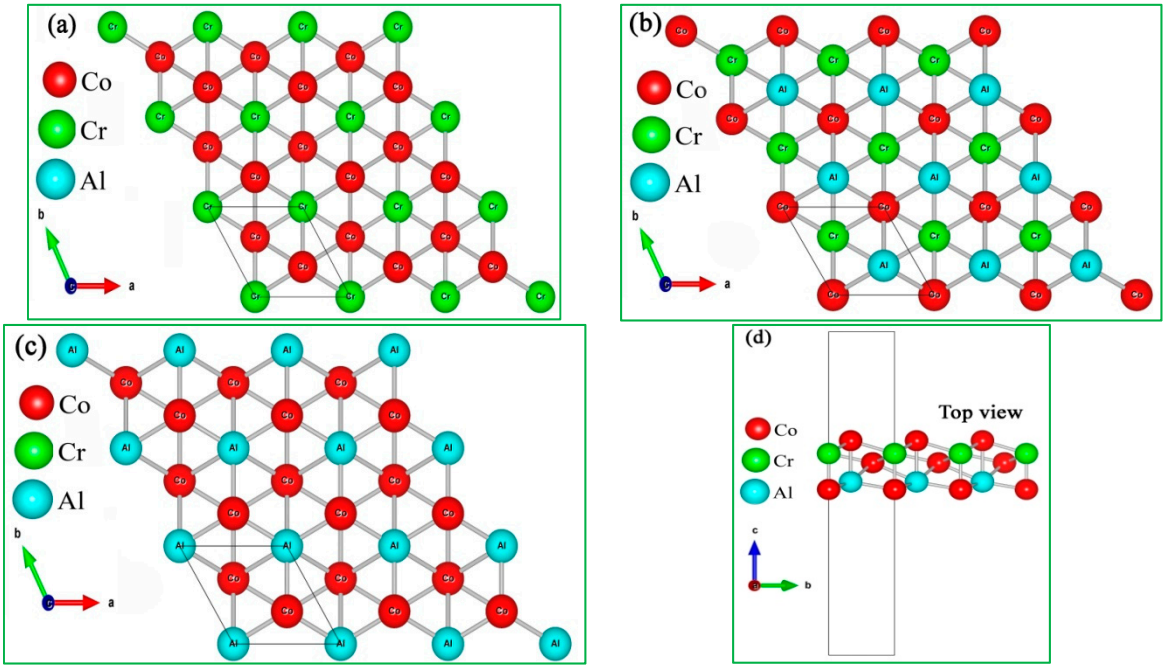


Figure 1. Crystal structure of the Co_2CrAl compound from top and side view for: (**a**) α-, (**b**) β- and, (**c**) γ- phases (**d**) shows the thickness of the atomic layers from the side.

In order to maintain a system, the first step is to find equilibrium volume at minimum energy. The total energy of each system has been calculated by fitting it to the Brich-Mornaghan equation for different unit cell volumes and the results are summarized in energy-volume (*E-V*) plots of Figure 2. In these calculations, after finding the equilibrium volume and the ground state point by *E-V* curves, the atomic forces has been optimized up to 10^{-6} (a.u./dyn).

Panels (a)–(d) of this figure indicate symmetric outline with a minimum point which confirm the static stability of the all inspected forms. Comparing panels (a) and (b) illustrates similarity between the *E-V* curves of the bulk state and α phase. Also, β and γ phases are similar. In the β phase, the slope of the curve increases with decreasing volume (under stress) which indicates more resistivity of this plane, while for other two planes, the curves are relatively symmetric on both sides of the equilibrium point. More curvature and slope in the *E-V* curve means that bulk modulus of the composition is large. Among the Heuslerne phases, β phase has the greatest *E-V* curve slope and thus the highest amount of bulk modulus. Due to the presence of magnetic atoms, Co and Cr, in this compound, the *E-V* curves are calculated in both ferromagnetic and anti-ferromagnetic phases. It is evidently concluded from Figure 2 that all Heuslerne phases are more stable in the ferromagnetic state and hence, we continue the following calculations just based on ferromagnetism.

Resulted data of the *E-V* curves are listed in Table 1. Clearly, the lattice constant of Co_2VAl is in agreement with other reports. The magnetic moment of this compound is integer 3, in accordance with Slater-Pauli rule, implying that this compound is a suitable option for spintronic purposes. Besides, the bulk modulus (hardness) of the bulk phase of Co_2VAl is twice that of steel metal, suggesting its potential application for industrial tools and parts. Derivative of the bulk modulus coefficient of this material unveils whose atomic bonds are of ionic type, resulting in a high crystalline strength. Negative values of the formation energy (E_{form}) for all phases in the ferromagnetic (*FM*) and anti-ferromagnetic (*AFM*) modes show that they are all quite stable from the energy point of view. The following equation is used to calculate the E_{form}:

$$\mathrm{E_{form}} = E_{total}^{bulkorHeuslerene} - (N_{Co}E_{Co} + N_{Cr}E_{Cr} + N_{Al}E_{Al} \quad (1)$$

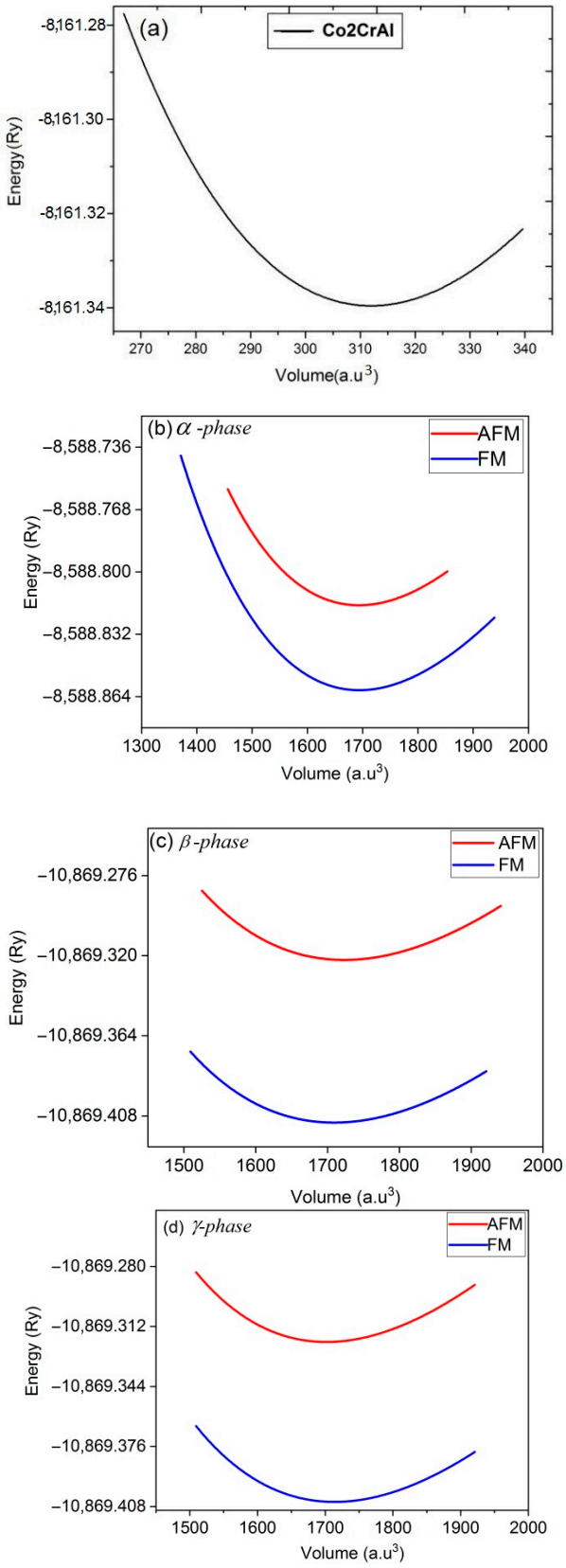


Figure 2. *E-V* curves of Co_2CrAl compound in the: (**a**) bulk, (**b**) α, (**c**) β and (**d**) γ Heuslerene phases. Minimum points approve that all structures are statically stable.

Table 1. Structural and mechanical properties of Co_2CrAl compound in the bulk and three Heuslerene phases, including: crystal lattice constants (a, c), formation energy (E_{for}), total magnetic moment (M_{tot}), partial magnetic moment (M_p), Bulk modulus (B), and derivative bulk modulus (B′).

Compound	a_0 (A°)	c/a (A°)	E_{for}(eV)	M_{tot} (μB)	M_p (μB)	B (GPa)	B'	*Energy* (Ry)
Co_2CrAl	5.701	—-	−0.377	3.00	—	204.9	5.00	
α-phase (*FM*)	7.15	3.75	−0.1858	0.00	Co: 0, Cr: 0, Al: 0	39.3	4.50	−8588.860
α-phase (*AFM*)	—-	—-	−0.8251	—-	—-	—-	—-	−8588.816
β-phase (*FM*)	7.54	3.75	−0.1742	1.00	Co_1: 0.45, Co_2: 0.31 Cr_1: 0.20, Cr_2:0.10, Al:0.0	41.6	4.51	−10,869.411
β-phase (*AFM*)	—-	—-	−0.8756	—-	—-	—-	—-	−10,869.322
γ-phase (FM)	7.50	3.75	−0.1750	7.15	Co_1:2.20, Co_2: 1.77 Co_3:1.41, Cr: 1.62, Al: 0.0	8.6	4.53	−10869.405
γ-phase (*AFM*)	—-	—-	−0.7985	—-	—-	—-	—-	−10,869.320

Which the $E_{total}^{bulkorHeuslerene}$, E_{Co}, E_{Cr}, and E_{Al} are the total energy of the bulk or Heuslerene unit cell, and energies of the Co, Cr, and Al crystals, respectively.

The lattice constants of the three Heuslerene phases are very close to each other, indicating their structural similarity, although they are different in the arrangement of their atoms, as shown in Figure 1. The Co_2VAl-β Heuslerene magnetic moment is an integer, 1, implying that it could be used in the spintronic industry. The bulk modulus of these 2D structures show that, due to their low thickness (a few atomic layers), they have suitable degree hardness. Also, their bulk modulus derivative verifies the existence of strong ionic bonds between their atoms. The magnetic moment in the β and γ phases have shown correct values, the partial magnetic moments have also shown that in the γ structure, we are facing a significant increase in the magnetic property of atoms and this two-dimensional structure.

3.1.2. Elastic Stabilities

Elasticity refers to the retrieval of the original shape of materials after removing applied force. Hence, the amount of elastic constants can specify structural stability and can create a connection between the atomic and large scales in order to predict important parameters such as hardness, brittleness/ductility nature, melting temperature, type of bonds, stiffness, and etc [67]. These parameters can provide valuable information about the practical applications.

The theoretical background of the elastic constants along with the calculation of parameters such as bulk modulus, shear modulus, Debye temperature, and … for bulk materials with different symmetry have been reported in our previous reports [63,64,67–69]. Moreover, as represented in our recent work [56], the theoretical background of the elastic constants for 2D materials as well as their appropriate amounts for the Heuslerene Ti_2VGe were investigated by using IRelast2D package [56,70] which worked as an interface with Wien2k code [71]. It should be noted that the experimental investigation of the elastic constants of 2D materials is a challenge for scientists at present [72] and so, such a package (IRelast2D) might be the best alternative which opens a new theoretical way for investigating the mechanical properties of 2D systems.

Mechanical parameters revealed the fact that when the percentage of *B*/*S* ratio of bulk material is less/more than 175%, it is brittle/ductile [73]. The Cauchy pressure sign is defined as (C_{12}-C_{44}) and specifies the sort of bonds. Commonly, the dominance of covalent or ionic bonds makes the sign of the bulk material's Cauchy pressure to be negative or positive, respectively [74]. Moreover, Poisson's ratio determines the bond type, so that for materials with covalent (ionic) bonds it is less than 0.25 (close to 0.25 or more) [68].

Stiffness is the resistivity of the matter in reaction to an applied force so that a stiff material has a higher Young's modulus and a flexible material has less stiffness. Hence, higher values of Young's modulus are essential when deflection is disagreeable. Hardness, as another important parameter, describes the resistivity of the matter to the shape variations. Among three parameters that indicate hardness i.e., shear modulus, bulk modulus, and Vickers hardness, better results can be achieved by characterizing the Vickers hardness [68] which can be calculated by following equations provided by Chen [75] and Tian [76]:

$$H_V^{Chen} = 2\left(k^2 S\right)^{0.585} - 3 \ \ \left(k = \frac{S}{B},\ \mathrm{S:shear},\ \mathrm{B:bulkmodulus}\right) \quad (2)$$

$$H_V^{Tian} = 0.92 k^{1.137} S^{0.708}$$

In the case of some ionic compounds for which Chen's equation detects negative values, Tian's equation reformulates it to solve this problem [76]. To evaluate thermodynamic parameters like Debye temperature (θ_D) as well as transversal (V_t), longitudinal (V_l), average (V_m) sound velocities, the Hill scheme is applied as an intermediate to the Voigt and Reuss model [67]. Table 2 includes the elastic constants, mechanical and thermodynamic parameters of the bulk Co_2CrAl in comparison with the previous theoretical reports [77,78] using the same methods and exchange-correlation (FP-LAPW-PBE) [79,80]. Our ab initio results are in agreement with previous theoretical calculations. The value of Poisson's ratio affirms that the dominant bonds are ionic which is compatible with our deduction from the positive sign of Cauchy pressure. The percentage of $\left(\frac{B_H}{S_H}\right)$ ratio for the bulk shape is 214% from which the ductile nature is inferred. The values of Vickers Hardness, based on Chen's and Tian's equations, are positive and almost close to each other. The elastic stability criterion (known as Born stability conditions) emerges when elastic energy of the compound is positive. From the mathematical standpoint, it is held when eigenvalues of the elastic constants matrix ($\boldsymbol{C}$) are positive [81,82]. For cubic symmetries, we have:

$$C_{11} - C_{12} > 0, C_{11} + 2C_{12} > 0, C_{44} > 0 \quad (3)$$

Our results show that bulk Co_2CrAl is mechanically stable and passes the elastic stability test.

The mechanical behavior of materials depends on their dimension and geometry [83–89]. Therefor, the physical behavior changes when we move from the bulk scale towards two- or one-dimensional scales. Table 3 represents the results gained by the IRelast2D package and PBE exchange-correlation for the elastic constants (C_{ij}), shear moduli (S), Young's moduli (Y), and Poisson's ratios (v) of the Co_2CrAl-X Heuslerenes where X = {Al (α-phase), Cr (β-phase), Co (γ-phase)} stands for the extra atom which resides at (0,0,0) as shown in Figure 1.

We should recall that, as far as we know, no experimental or theoretical reports have been published about the 2D Co_2CrAl yet. The directional values of Young's moduli in Table 3 show that three Heuslerene phases of Co_2CrAl are isotropic along the x and y directions. Also, their Young's moduli are less than bulk form, meaning that all these Heuslerenes are of less stiffness than bulk. However, the α-phase has greater amounts of Y and thus, is stiffer than β and γ phases. Shear modulus (ratio of shear stress to shear strain), which is the representative of hardness, describes the resistance of the material to the shape changes. Hence, Co_2CrAl-Al is harder than other two Heuslerenes. The hardness decreases when we move from the bulk towards the surface.

Table 2. The values of elastic constants (C_{ij} in (GPa)), Bulk moduli (B), shear moduli (S), and Young's moduli (Y) in GPa in the Voigt-Reuss-Hill (VRH) approximation, Poisson's ratios (ν), as well as transverse (V_t), longitudinal (V_L) and average wave velocities (V_m in m/s), Debye temperature (Θ_D in (K)) and Vickers hardness base on the Chen and Tian equations (H_V in (GPa)) for the bulk form of Co_2CrAl.

CUBIC	Co_2CrAl	Co_2CrAl [a]	Co_2CrAl [b]
C_{11}	274.85	**265.0**	**278.07**
C_{12}	180.12	**196.2**	**187.94**
C_{44}	161.69	**156.1**	**151.91**
B_V	211.70	**201.5**	
B_R	211.70	**201.5**	
B_H	211.70	**201.5**	
S_V	115.96		
S_R	82.26		
S_H	99.11	**97.2**	
Y_V	294.17		**280.66**
Y_R	218.49		**208.98**
Y_H	257.20	**251.3**	**245.57**
ν_V	0.268		
ν_R	0.327		
ν_H	0.297	0.29	
V_T	3743.71		
V_L	6973.03		
V_m	4180.32		
Θ_D	550.50		
$H_V{}^{Chen}$	9.11		
$H_V{}^{Tian}$	10.05		

Previous theoretical results are bold. [a]: Ref. [77] (PBE). [b]: Ref. [78] (PBE).

Table 3. The values of elastic constants (C_{ij} in (N/m)), shear moduli (S), and Young's moduli (Y) in N/m and Poisson's ratios (ν) for three Heuslerene phases of Co_2CrAl.

Material	C_{11}	C_{22}	C_{12}	C_{66}	Y_x	Y_y	S_{xy}	ν_{xy}	ν_{yx}	Elastically Stable
α-phase	120.36	120.36	52.36	33.92	97.55	97.55	33.99	0.44	0.44	✓
β-phase	97.30	97.30	47.65	24.83	73.97	73.97	24.83	0.49	0.49	✓
γ-phase	95.52	95.52	48.86	23.33	70.52	70.52	23.33	0.51	0.51	✓

As another result, all Poisson's ratios of the Heuslerenes are positive, with largest value for the γ-phase, and independent of the x and y directions. With reference to Table 3, the largest and smallest amounts of the elastic parameters, including C_{11}, C_{22}, C_{66}, Y_x, Y_y, and S_{xy} belong to the α and γ phase, respectively, while for the Poisson's ratio an inverse behavior is observed. Obviously, Co_2CrAl-Al is mechanically stronger than other two Heuslerene phases, since its elastic constants (C_{11}, C_{12} and C_{66}) are larger. From the viewpoint of elasticity, all phases pass the elastic stability test and hence, they are mechanically stable.

3.1.3. Phonon Stability

Having proved the static stability of the bulk and three Heuslerene shapes of Co_2CrAl, it is essential to investigate their dynamical stability as well. For this aim, the phonon BSs in Figure 3a–d, which concerns the crystal vibrations over the first Brillouin zone, is analyzed. All frequency branches in these plots are positive implying that all discussed phases of Co_2CrAl are dynamically stable. For the bulk phase, steeper acoustical branches around Γ point infer the transformation of thermal energy in the 0–200 cm^{-1} region and so, it may act as a good heat conductor along this direction. However, in the range of 200–270 cm^{-1} and 310–390 cm^{-1} two big optical gaps are observed and their optical branches have low slope and are nearly flat, so that the IR energy with low mobility accumulates in this region.

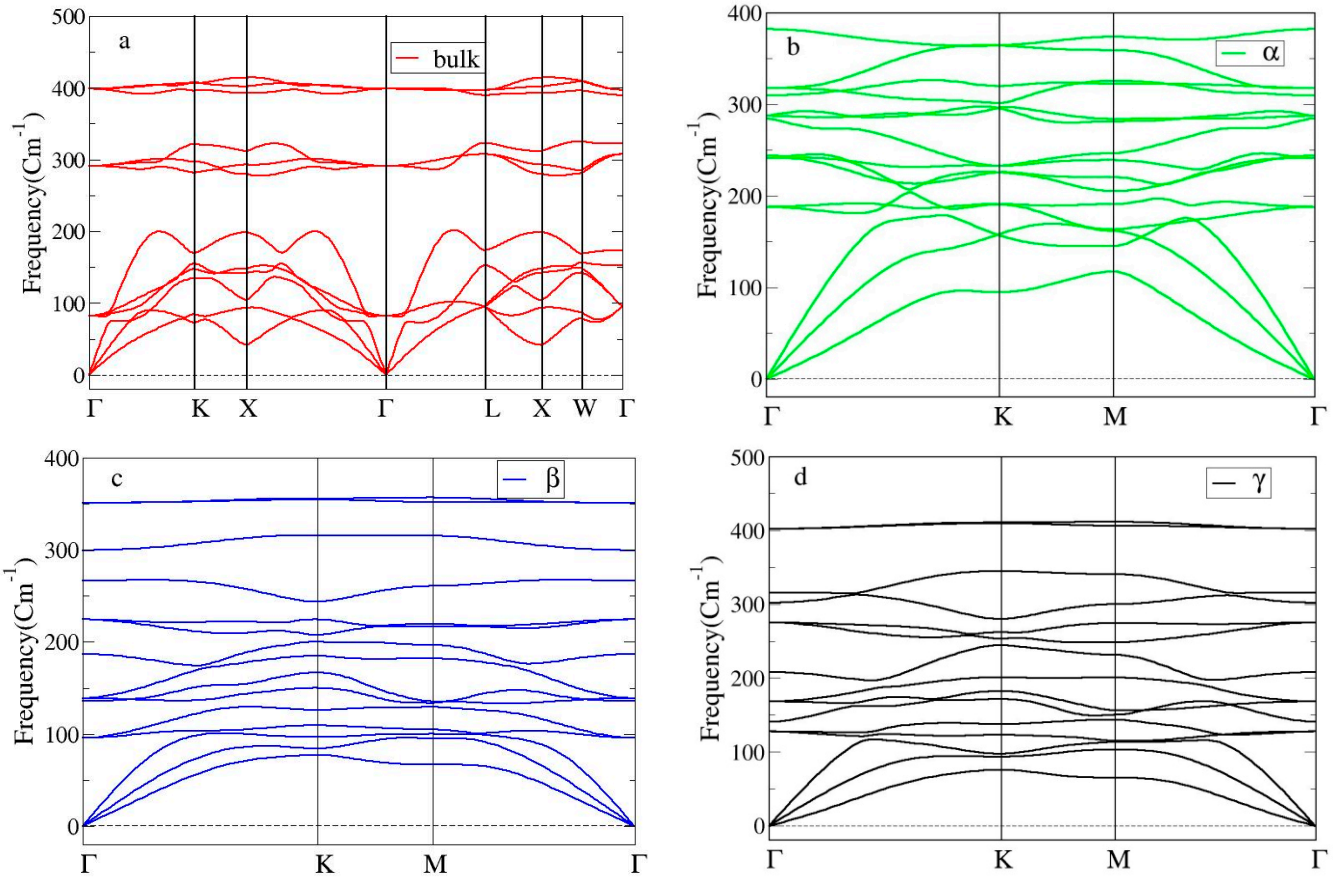


Figure 3. Phonon *BSs* of Co_2CrAl in four different phases: (**a**) Bulk, (**b**) α-, (**c**) β-, and (**d**) γ-Heuslerene shapes.

Moreover, Figure 3b–d shows that all three 2D predicted forms of Co_2CrAl are strongly stable against the lattice vibrations. These figures are plotted along the -Γ*K*-*M*-Γ path within the first Brillouin zone. The acoustical branches of these Heuslerenes have a higher slope than optical branches. This is particularly observed in the α case where the slope of acoustical branches around the Γ point is more and thus, this structure can better convey the low-frequency thermal energies. There are three phonon band gaps for the β case and one phonon band gap for the γ case observed in the range of frequencies more than 240 cm^{-1} and 340–400 cm^{-1}, respectively. Because of qualitative similarity between the phonon BSs of the bulk and β phases (such as the ranges of optical gaps), more similarity in their optical behavior is expected. Further, among these 2D structures, the highest energy level (~400 cm^{-1}) belongs to the γ case which is still a bit lower than that of the bulk shape. This means that any change in the type and arrangement of the comprising atoms may

result in changes in the energy levels and thus optical behavior (including IR conductivity) of the ultimate compound.

3.1.4. Phase Stability Diagrams Stability

The phase diagram of any compound evaluates all possible formations by considering the Gibbs energies. Figure 4 displays the phase diagram of the bulk Co_2CrAl based on the following formula for its Gibbs energy:

$$2\mu_{Co} + \mu_{Cr} + \mu_{Al} = g^{bulk}_{Co2CrAl} \quad (4)$$

where μ_{Co}, μ_{Cr}, and μ_{Al} are chemical potentials of the comprising atoms. The accessible area which satisfies this equation is considered as the allowed region and its borders are determined by following equations:

$$1/2(G_{Co2CrAl} - G_{CrAl}) \leq \Delta\mu_{Co} \leq G^{bulk}_{Co} \quad (5)$$

$$G_{Co2CrAl} - G_{Co2Al} \leq \Delta\mu_{Cr} \leq G^{bulk}_{Cr} \quad (6)$$

$$G_{Co2CrAl} - G_{Co2Cr} \leq \Delta\mu_{Al} \leq G^{bulk}_{Al} \quad (7)$$

in these relations, $\Delta\mu_i$ is the chemical potential change of atom i and their ideal amounts are $\Delta\mu_i \geq 0$ which means that changes are assumed to be between their maximum and minimum values. The minimum value of μ_i is found where atom i departs from the compound and its maximum value refers to crystallization of atom i in its bulk form with the Gibbs energy of g^{bulk}_i.

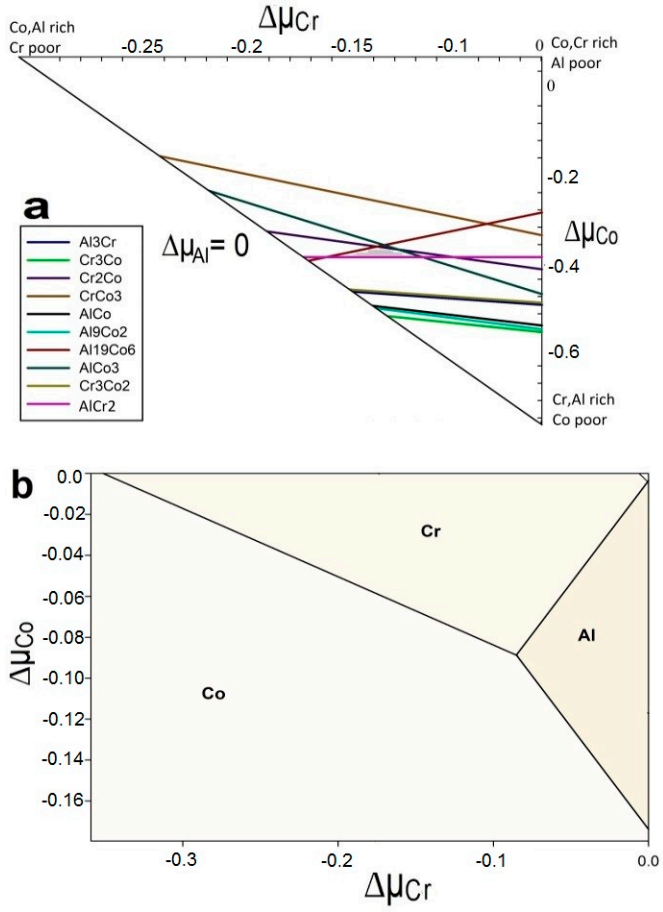


Figure 4. The stability phase diagrams of Co_2CrAl in the (**a**) bulk, and (**b**) Heuslerene phases. Chemical potential changes are expressed in Rydberg unit.

Each corner in the triangle of Figure 4a corresponds to a point where one of the atomic components of Co_2CrAl leaves the structure. In other words, each corner fits the chemical potential of a specific type of atom. Therefore, the chemical potential of Al atom has been fixed and over the whole range of changes in other chemical potentials, the free Gibbs energies for a variety of possible combinations of Co, Cr, and Al have been plotted. Some triangles may emerge from the intersection of these lines but one of them, which is marked as a hachured area, illustrates the region where the three atoms can be simultaneously present in Co_2CrAl with space group of $Fm\bar{3}m$. The phase diagrams for all three Heuslerene phases are compared is Figure 4b by calculating the surface free energies of these 2D structures through the following equation:

$$\gamma_i(T, P_i) = G^{slab} - \sum_i N_i \mu_i \quad (8)$$

In which, G^{slab} is the surface Gibbs energy. μ_i and N_i are chemical potential and number of atoms in supercell. P_i and T are also the partial pressure and temperature of the components, respectively. For our 2D systems, this equation can be rephrased as below:

$$\gamma_i(T,P_i) = G^{slab} - \mu_{Co}N_{Co} - \mu_{Cr}N_{Cr} - \mu_{Al}N_{Al})/2A \quad (9)$$

In which, the factor 2 in denominator of the right side is due to the two similar surfaces on both sides of the layer, and A is the surface area. The accessible region in this case can be found from Equations (4)–(6). All 2D shapes of Co_2CrAl in Figure 4b lie into the allowed area of stability, with belonging the biggest and smallest area to the γ and α phase, respectively. Therefore, all these Heuslerenes of Co_2CrAl are likely to be synthesized in the lab under suitable conditions.

3.2. Electronic Properties

The *DOS* curves of the above-mentioned phases of Co_2CrAl for both up and down spin distributions are illustrated in Figure 5a–d. Panel (a) shows that in the bulk form, the spin-up electronic states have overlapped over the whole positive and negative energies and cut the Fermi level, suggesting a strong metallic nature. However, for the spin-down channel, a p-type semiconductor outline is observed whose values of the energy gap and spin-flip gap are 0.64 eV and 0.14 eV, respectively. In half-metallic compounds and in minority spins, the distance from the Fermi level to the edge of electronic states is called spin-flip gap, and is obtained based on Kohn-Sham equations as follows [90]:

$$E_{KS}^{sf+} = \varepsilon_{L\uparrow} - \varepsilon_{H\downarrow} \quad (10)$$

$$E_{KS}^{sf-} = \varepsilon_{L\downarrow} - \varepsilon_{H\uparrow} \quad (11)$$

In which $\varepsilon_{L\uparrow}$ ($\varepsilon_{L\downarrow}$) is the upper (lower) energy of unoccupied orbitals and $\varepsilon_{H\uparrow}$ ($\varepsilon_{H\downarrow}$) is the upper (lower) energy of occupied orbitals.

Consequently, the bulk phase of Co_2CrAl is a half-metal with the magnetic moment of 3 μB and 100% spin polarization at the Fermi level, which makes it applicable in spintronics and spin injection applications. Plotted in panels (b–f) of Figure 5 are the electronic *DOS* of the 2D phases for the majority and minority spins using GGA, GGA+U, and GGA+U+mBJ approximations. It is evident that *DOS* curves of all Heuslerene phases, in comparison to the bulk, are more serrated, owing to their nano-scale entity and the important role of free electrons on their surfaces. The α and γ phases seem to be metal for both spin directions in all imposed approximations, however, they exhibit the most anisotropy by GGA+U+mBJ. Salient is the β phase which exhibits different magnetic properties for different approximations. For the region of −3 eV to 2 eV, it is magnetically anisotropic in GGA, isotropic in GGA+U, but extremely anisotropic at the Fermi level in GGA+U+mBJ. In the last case, the β phase is a p-type semiconductor with 0.27 eV energy gap for spin-up. But for spin-down, a strong metal with a continuous spectrum of states is observed. In

Figure 5, the partial *DOS* curve of the β phase with GGA+U+mBJ approximation is plotted for both up and down spins. It is observable that below and above the Fermi level, *d* orbital of the Cr atom has the highest value and is the main reason for conduction and transport of the electrons and holes. Overlap of the *d* orbitals of Cr and Co with *p* orbitals of Al in the energy range of −0.5 eV to −3.5 eV gives rise to the *d*-*d* and *p*-*d* bonds.

For more details, the electronic *BS* of the aforementioned phases of Co_2CrAl have been calculated and plotted in Figure 6. Clearly, for minority spins, the bulk phase is a p-type semiconductor with the direct gap of 0.64 eV around the Γ point, which is compatible with the *DOS* results and other reports. However, for majority spins, high slope of the conduction bands with energies more than 1 eV, is a testament to the enormous mobility of the related electrons, which is due to the relationship of group velocity $\left(E_g = \frac{1}{\hbar}\frac{\partial E}{\partial K}\right)$ and effective mass $\left(m^* = \frac{1}{\frac{1}{\hbar^2}\frac{\partial^2 E}{\partial K^2}}\right)$ to the first derivative and the second derivative of energy relative to the momentum vector. For β case, two spin-up electronic bands meet the Fermi level, as expected, and an indirect band gap appears within the spin-down bands. Here, the maximum valance band and minimum conduction band are placed at Γ and *K* points, respectively. The large gradient of the electronic states is remarkable in the conduction domain, from which a huge degree of electronic mobility can be inferred. The difference between the *BS* profiles of the up and down spin channels means that the thermodynamic behavior of this Heuslerene compound can be adjusted by an external field.

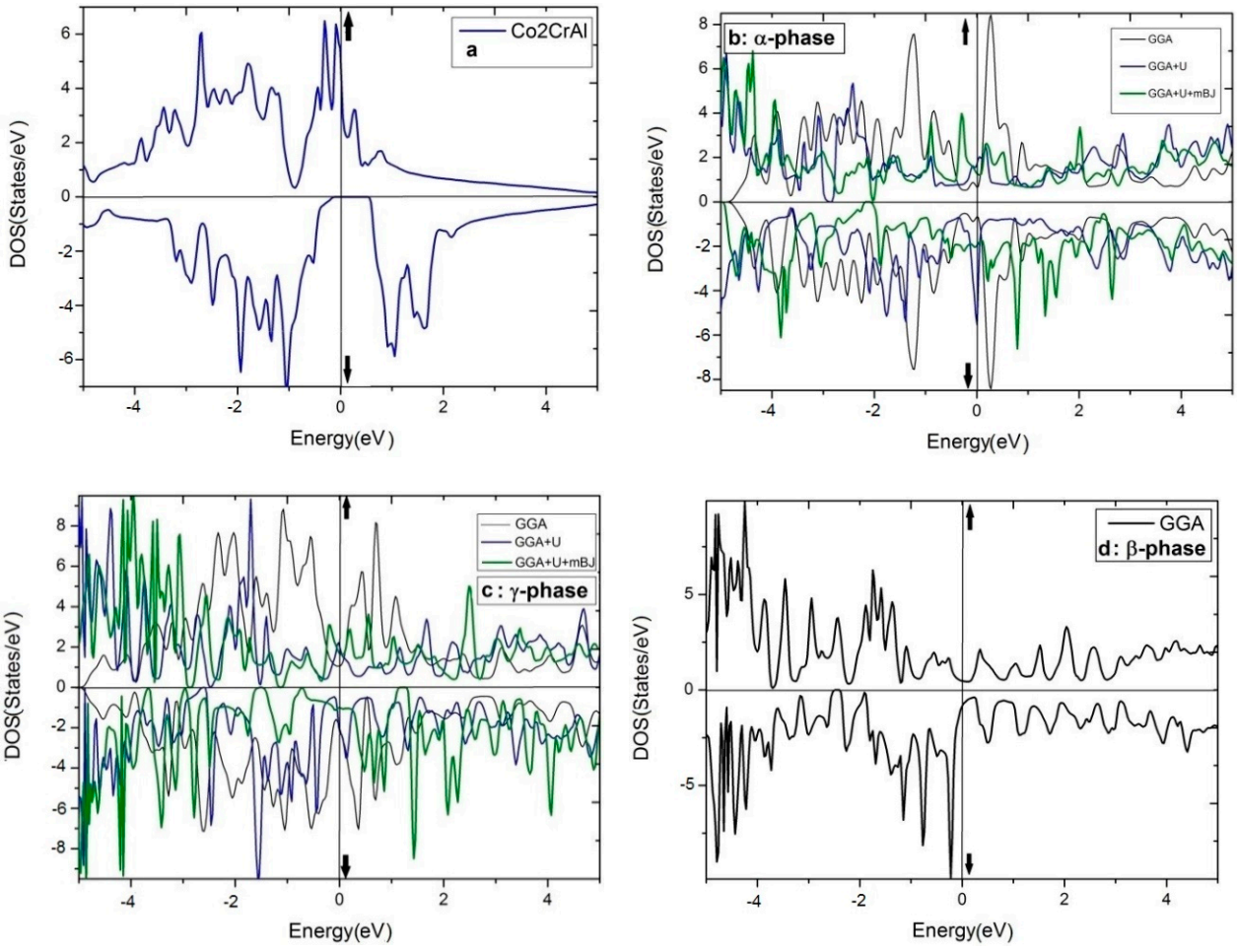


Figure 5. *Cont.*

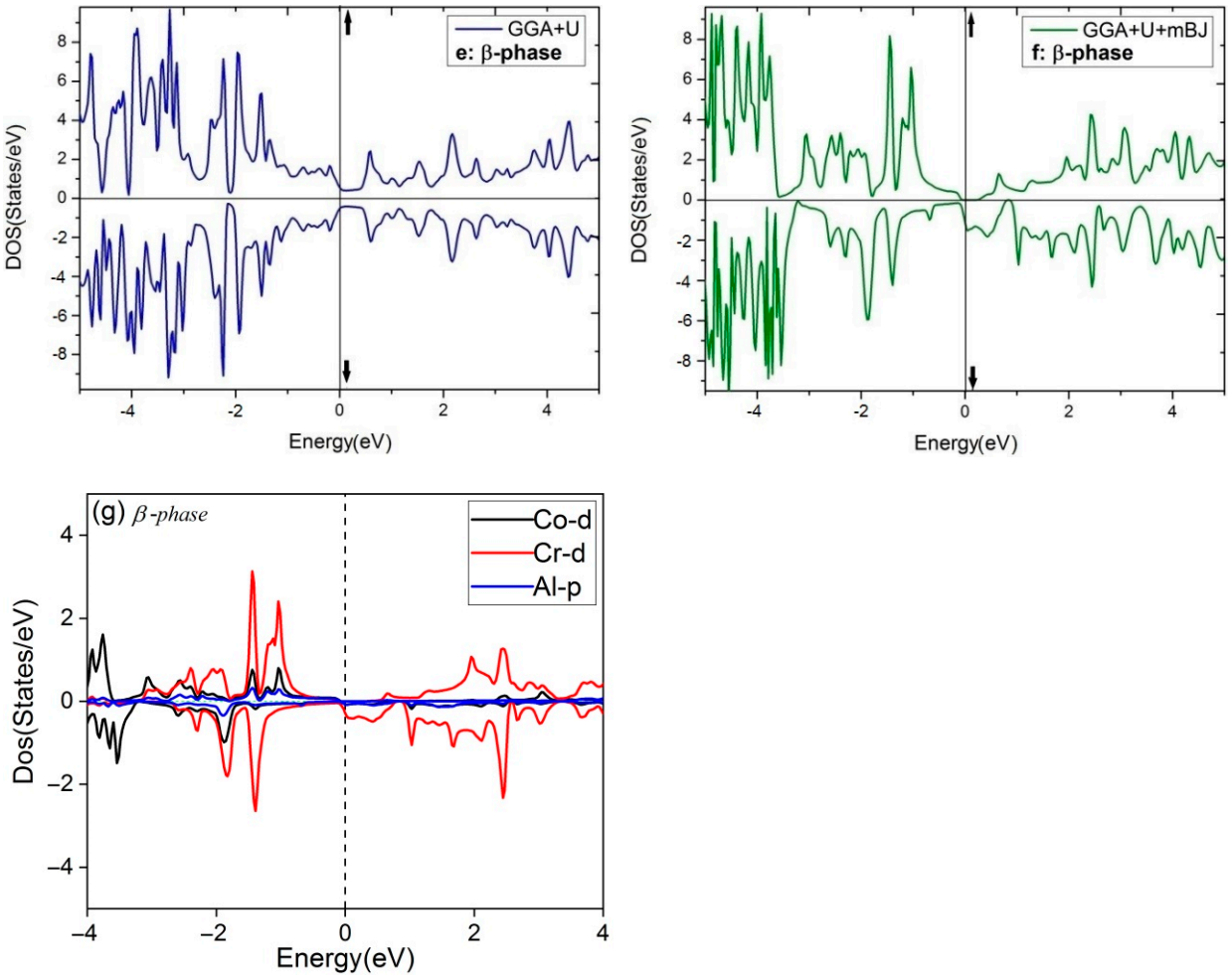


Figure 5. The total DOS of four phases of Co_2CrAl for three different approximations: (**a**) Bulk phase, (**b**) α phase, (**c**) γ phase, (**d**) β phase by GGA, (**e**) β phase by GGA+U, (**f**) β phase by GGA+U+mBJ, and (**g**) The Partial DOS of β phase by GGA+U+mBJ.

In Figure 7, electron density diagrams are plotted on the Heuslerene Co_2CrAl plates. It is clear that Al, Cr and Co atoms are present at the surface of the α, β and γ phases, respectively. The presence of electron density and dangling bonds on the surface of films and 2D structures gives rise to new physical properties in them. According to the figures, the highest presence of electron density occurs at the α phase, and the lowest at β case. The magnitude of electron density in the α phase relative to β one is in the order of ten. Accumulation of electron density at the α and γ phases have caused them to exhibit strong metallic properties. On the other hand, presence of Cr atoms in the surface of the β phase causes more polarization of the electron density than other two phases. Besides, this electron density is due to half-full *d*-orbitals that have given a magnetic behavior to the electronic properties of this phase. As we saw in Table 1, the magnetic moment of this phase is the integer 1.0 μB. Therefore, the presence of more free electrons in the two-dimensional structure of α and γ phases have increased the metallic behavior in them, and in the β phase, we saw full half-metallic behavior with controllable magnetic behavior.

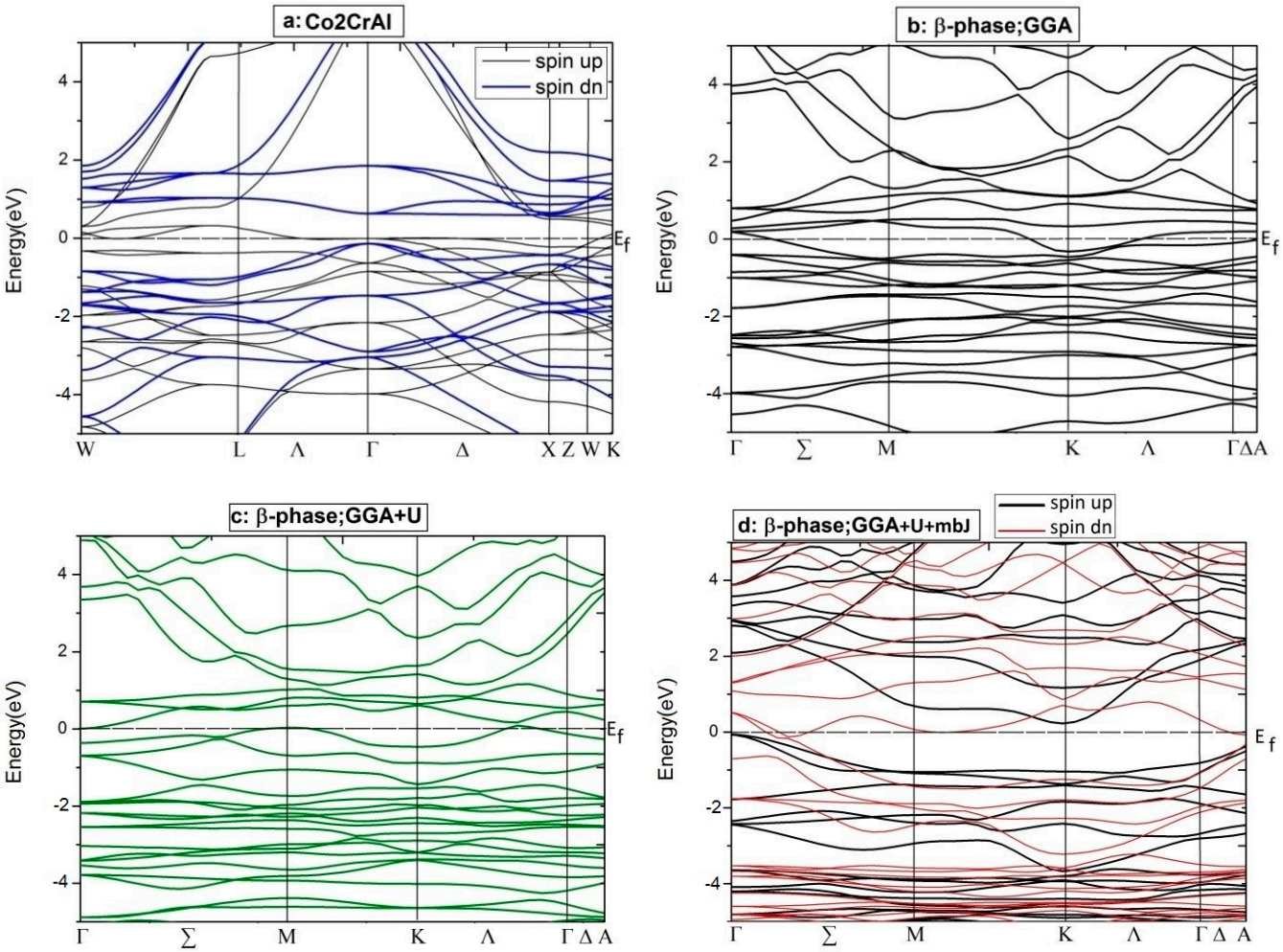


Figure 6. Electronic BSs for two spin distributions of just two phases of Co_2CrAl: (**a**) Bulk phase by GGA (**b**) β phase by GGA, (**c**) β phase by GGA+U, and (**d**) β phase by GGA+U+mbJ.

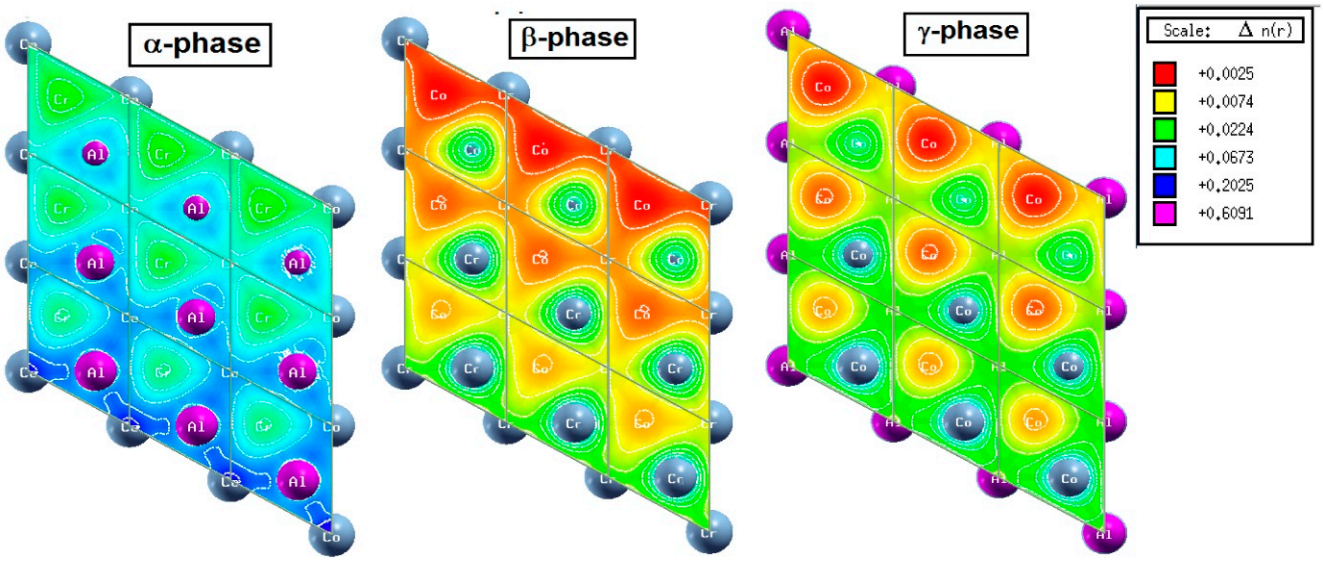


Figure 7. Three Heuslerene monolayers of Co_2CrAl, named α, β and γ. The difference arises from the termination of the surface atoms.

4. Conclusions

The *F.C.C* structure of the Heusleres provides a compact arrangement of atoms along their [111] direction and hence, the thin films and 2D structures extracted by cutting the bulk form in this direction may be of high compactness and stability. In this work, Heuslerenes were expanded to the novel 2D structures by introducing a new member based on Co_2CrAl and dealing with its expected properties in details. The crystal elastic constants for the bulk structure are obtained using the method proposed by Jamal in the Wien2K framework.

The structural stability was estimated by amounts of the elastic constants. Also, thermodynamic characteristics were evaluated by Hill scheme as an intermediate to the Voigt and Reuss evaluations. Our ab initio results are in good agreement with previous theoretical calculations. The value of Poisson's ratio confirmed the ionic dominant bonds which is compatible with our deduction from the positive sign of Cauchy pressure. Besides, the ductile nature was inferred from the percentage of $\left(\frac{B_H}{S_H}\right)$ ratio in bulk Co_2CrAl which was 214%. The values of Vickers Hardness, based on Chen's and Tian's equations, were positive and almost close to each other. The directional values of Young's moduli revealed the isotropic nature of all three Heuslerene phases of Co_2CrAl along the $\boldsymbol{x}$ and $\boldsymbol{y}$ directions. Moreover, while moving from bulk scale towards the sheet, hardness decreased. Comparing to other Co_2CrAl Heuslerene phases, the elastic constants (C_{11} and C_{12} and C_{66}) of Co_2CrAl-Al were larger and hence, it was mechanically stronger. The positive value of all frequency branches of phonon distribution diagrams implied that all phases of Co_2CrAl were dynamically stable. Also, all 2D predicted forms of Co_2CrAl were strongly stable against the lattice vibrations.

According to our phase diagram calculation for the bulk shape, a hachured area illustrated the region where all three atoms could be simultaneously placed in Co_2CrAl with the space group of $Fm\bar{3}m$. All 2D phases of Co_2CrAl lied into the allowed area of stability and the biggest and smallest area belonged to the γ and α phase, respectively.

Moreover, the half-metallic nature of the bulk phase was demonstrated by extracting its electronic structure. Besides, the value of magnetic moment and the percentage of spin polarization at the Fermi level were 3 μ_B and 100%, respectively, meaning that it could be employed for spintronics and spin injection applications. α and γ phases seemed to be metal in both spin directions and all approximations but the most anisotropy was exhibited in the GGA+U+mBJ approximation. Finally, β phase was noticeable for exhibiting different magnetic properties in different approximations, such that in the -3 eV to 2 eV region, it was magnetically anisotropic in GGA, but isotropic in GGA+U, and extremely anisotropic at the Fermi level in GGA+U+mBJ. Also, it was a p-type semiconductor with a 0.27 eV energy gap for spin-up, but a strong metal with a continuous spectrum of states for spin- down. As a prospect, mechanical exfoliation, as the most popular methods to extract 2D materials from bulk crystals, may be applied to bring this Heuslerene structure into existence.

Author Contributions: Conceptualization, A.B. and S.S.; methodology, A.B.; software, M.A. (Moein Asshabi), J.K., E.S. and M.J.; validation, J.S., M.S. and M.A. (Malieheh Amiri); formal analysis, A.Y.; writing—original draft preparation, A.h.S. and S.J.-A.; writing—review and editing, A.B., M.A. (Moein Asshabi), J.K. and E.S.; visualization, S.S.; supervision, A.B.; project administration, J.S., and M.S.; funding acquisition, No fund. All authors have read and agreed to the published version of the manuscript.

Funding: This research received no external funding.

Data Availability Statement: Our data is not supported outside the computing team and the results are completely original.

Conflicts of Interest: The authors declare no conflict of interest.

References

1. Amudhavalli, A.; Rajeswarapalanichamy, R.; Iyakutti, K. Half metallic ferromagnetism in Ni based half Heusler alloys. *Comput. Mater. Sci.* **2018**, *148*, 87–103. [CrossRef]
2. Amudhavalli, A.; Rajeswarapalanichamy, R.; Iyakutti, K. Structural, electronic, mechanical and magnetic properties of Mn based ferromagnetic half Heusler alloys: A first principles study. *J. Alloys Compd.* **2017**, *708*, 1216–1233. [CrossRef]
3. Casper, F.; Graf, T.; Chadov, S.; Balke, B.; Felser, C. Half-Heusler compounds: Novel materials for energy and spintronic applications. *Semicond. Sci. Technol.* **2012**, *27*, 063001. [CrossRef]
4. Hamaya, K.; Yamada, M. Semiconductor spintronics with Co2-Heusler compounds. *MRS Bull.* **2022**, *47*, 584–592. [CrossRef]
5. Patel, P.D.; Pandya, J.B.; Shinde, S.M.; Gupta, S.D.; Narayan, S.; Jha, P.K. Investigation of Full-Heusler compound Mn2MgGe for magnetism, spintronics and thermoelectric applications: DFT study. *Comput. Condens. Matter* **2020**, *23*, e00472. [CrossRef]
6. Berarma, K.; Essaoud, S.S.; Mousa, A.A.; Azar, S.M.; Al-Reyahi, A.Y. Opto-electronic, thermodynamic and charge carriers transport properties of $Ta_2FeNiSn_2$ and $Nb_2FeNiSn_2$ double half-Heusler alloys. *Semicond. Sci. Technol.* **2022**, *37*, 055013. [CrossRef]
7. Kumar, A.; Singh, P.K.; Sadiq, M.; Singh, R.P. A first principle study of magnetic and opto-electronic properties of half metallic Heusler alloy, Co_2TiSi. *Mater. Today Proc.* **2021**, *47*, 1605–1609. [CrossRef]
8. Sakuraba, Y.; Kokado, S.; Hirayama, Y.; Furubayashi, T.; Sukegawa, H.; Li, S.; Takahashi, Y.K.; Hono, K. Quantitative analysis of anisotropic magnetoresistance in Co_2MnZ and Co_2FeZ epitaxial thin films: A facile way to investigate spin-polarization in half-metallic Heusler compounds. *Appl. Phys. Lett.* **2014**, *104*, 172407. [CrossRef]
9. Nikolaev, K.; Kolbo, P.; Pokhil, T.; Peng, X.; Chen, Y.; Ambrose, T.; Mryasov, O. "All-Heusler alloy" current-perpendicular-to-plane giant magnetoresistance. *Appl. Phys. Lett.* **2009**, *94*, 222501. [CrossRef]
10. Webster, P.J.; Ziebeck, K.R.A. Magnetic and chemical order in Heusler alloys. Containing cobalt and titanium. *J. Phys. Chem. Solids* **1973**, *34*, 1647–1654. [CrossRef]
11. Kübler, J.; William, A.R.; Sommers, C.B. Formation and coupling of magnetic moments in Heusler alloys. *Phys. Rev. B* **1983**, *28*, 1745–1755. [CrossRef]
12. De Groot, R.A.; Mueller, F.M. New Class of Materials: Half-Metallic Ferromagnets. *Phys. Rev. Lett.* **1983**, *50*, 2024–2027. [CrossRef]
13. Hirohata, A.; Yamada, K.; Nakatani, Y.; Prejbeanu, I.-L.; Diény, B.; Pirro, P.; Hillebrands, B. Review on spintronics: Principles and device applications. *J. Magn. Magn. Mater.* **2020**, *509*, 166711. [CrossRef]
14. Ishida, S.; Akazawa, S.; Kubo, Y.; Ishida, J. Band theory of Co_2MnSn, Co_2TiSn and Co_2TiAl. *J. Phys. F Met. Phys.* **1982**, *12*, 1111. [CrossRef]
15. Tong, B.Y.; Sham, L.J. Application of a Self-Consistent Scheme Including Exchange and Correlation Effects to Atoms. *Phys. Rev.* **1966**, *144*, 1. [CrossRef]
16. Hedin, L.; Lundqvist, B.I. Explicit local exchange-correlation potentials. *J. Phys. C Solid State Phys.* **1971**, *4*, 2064–2083. [CrossRef]
17. Von Barth, U.; Hedin, L. A local exchange-correlation potential for the spin polarized case. *J. Phys. C Solid State Phys.* **1972**, *5*, 1629–1642. [CrossRef]
18. Vosko, S.H.; Wilk, L.; Nusair, M. Accurate spin-dependent electron liquid correlation energies for local spin density calculations: A critical analysis. *Can. J. Phys.* **1980**, *58*, 1200–1211. [CrossRef]
19. Ishida, S.; Fujii, S.; Kashiwagi, S.; Asano, S. Search for Half-Metallic Compounds in Co_2MnZ (Z=IIIb, IVb, Vb Element). *J. Phys. Soc. Jpn.* **1995**, *64*, 2152–2157. [CrossRef]
20. Ishida, S.; Kashiwagi, S.; Fujii, S.; Asano, S. Magnetic and half-metallic properties of new Heusler alloys Ru_2MnZ (Z = Si, Ge, Sn and Sb). *Phys. B Condens. Matter* **1995**, *210*, 140–148. [CrossRef]
21. Mohn, P.; Blaha, P.; Schwarz, K. Magnetism in the Huesler alloys: Co_2TiSn and Co_2TiAl. *J. Magn. Magn. Mater.* **1995**, *140–144*, 183–184. [CrossRef]
22. Galanakis, I.; Dederichs, P.H.; Papanikolaou, N. Slater-Pauling behavior and origin of the half-metallicity of the full-Heusler alloys. *Phys. Rev. B* **2002**, *66*, 174429. [CrossRef]
23. Picozzi, S.; Continenza, A.; Freeman, A.J. Co_2MnX (X = Si, Ge, Sn) Heusler compounds: An *ab initio* study of their structural, electronic, and magnetic properties at zero and elevated pressure. *Phys. Rev. B* **2002**, *66*, 094421. [CrossRef]
24. Miura, Y.; Nagao, K.; Shirai, M. Atomic disorder effects on half-metallicity of the full-Heusler alloys $Co_2(Cr1-xFex)Al$: A first-principles study. *Phys. Rev. B* **2004**, *69*, 144413. [CrossRef]
25. Antonov, V.N.; Dürr, H.A.; Kucherenko, Y.; Bekenov, L.V.; Yaresko, A.N. Theoretical study of the electronic and magnetic structures of the Heusler alloys $Co_2Cr1-xFexAl$. *Phys. Rev. B* **2005**, *72*, 054441. [CrossRef]
26. Huang, H.L.; Tung, J.C.; Guo, G.Y. Anomalous Hall effect and current spin polarization in Co_2FeX Heusler compounds X=Al, Ga, In, Si, Ge, and Sn): A systematic *ab initio* study. *Phys. Rev. B* **2015**, *91*, 134409. [CrossRef]
27. Kübler, J.; Fecher, G.H.; Felser, C. Understanding the trend in the Curie temperatures of Co_2-based Heusler compounds: *Ab initio* calculations. *Phys. Rev. B* **2007**, *76*, 024414. [CrossRef]
28. Wang, Q.H.; Kalantar-Zadeh, K.; Kis, A. Electronics and optoelectronics of two-dimensional transition metal dichalcogenides. *Nat. Nanotechnol.* **2012**, *7*, 699–712. [CrossRef]
29. Zhou, F.; Cui, C.; Wang, J.; Kuang, M.; Yang, T.; Yu, Z.-M.; Wang, X.; Zhang, G.; Cheng, Z. Perovskite-type YRh_3B with multiple types of nodal point and nodal line states. *Phys. Rev. B* **2021**, *103*, 245126. [CrossRef]

30. Zhou, F.; Zhang, Z.; Chen, H.; Kuang, M.; Yang, T.; Wang, X. Hybrid-type nodal ring phonons and coexistence of higher-order quadratic nodal line phonons in an AgZr alloy. *Phys. Rev. B* **2021**, *104*, 174108. [CrossRef]
31. Zhang, G.; Zhang, Y.W. Thermoelectric properties of two-dimensional transition metal dichalcogenides. *J. Mater. Chem. C* **2017**, *5*, 7684–7698. [CrossRef]
32. Liu, K.; Wu, J. Mechanical properties of two-dimensional materials and heterostructures. *J. Mater. Res.* **2016**, *31*, 832–844. [CrossRef]
33. Schedin, F.; Geim, A.K.; Morozov, S.V.; Hill, E.W.; Blake, P.; Katsnelson, M.I.; Novoselov, K.S. Detection of individual gas molecules adsorbed on graphene. *Nat. Mater.* **2007**, *6*, 652–655. [CrossRef]
34. Blake, P.; Brimicombe, P.D.; Nair, R.R.; Booth, T.J.; Jiang, D.; Schedin, F.; Ponomarenko, L.A.; Morozov, S.V.; Gleeson, H.F.; Hill, E.W.; et al. Graphene-Based Liquid Crystal Device. *Nano Lett.* **2008**, *8*, 1704–1708. [CrossRef] [PubMed]
35. El-Kady, M.F.; Strong, V.; Dubin, S.; Kaner, R.B. Laser scribing of high-performance and flexible graphene-based electrochemical capacitors. *Science* **2012**, *335*, 1326–1330. [CrossRef] [PubMed]
36. Fowler, J.D.; Allen, M.J.; Tung, V.C.; Yang, Y.; Kaner, R.B.; Weiller, B.H. Practical Chemical Sensors from Chemically Derived Graphene. *ACS Nano* **2009**, *3*, 301–306. [CrossRef]
37. Bae, S.H.; Lee, Y.; Sharma, B.K.; Lee, H.J.; Kim, J.H.; Ahn, J.H. Graphene-based transparent strain sensor. *Carbon* **2013**, *51*, 236–242. [CrossRef]
38. Schwierz, F. Graphene transistors. *Nat. Nanotechnol.* **2010**, *5*, 487–496.
39. Sakhaee-Pour, A.; Ahmadian, M.T.; Vafai, A. Potential application of single-layered graphene sheet as strain sensor. *Solid State Commun.* **2008**, *147*, 336–340. [CrossRef]
40. Acun, A.; Zhang, L.; Bampoulis, P.; Farmanbar, M.; van Houselt, A.; Rudenko, A.N.; Lingenfelder, M.; Brocks, G.; Poelsema, B.; I Katsnelson, M.; et al. Germanene: The germanium analogue of graphene. *J. Condens. Matter Phys.* **2015**, *27*, 443002. [CrossRef]
41. Ozcelik, V.O.; Kecik, D.; Durgun, E.; Ciraci, S. Adsorption of Group IV Elements on Graphene, Silicene, Germanene, and Stanene: Dumbbell Formation. *J. Phys. Chem. C* **2015**, *119*, 845–853. [CrossRef]
42. Laniel, D.; Geneste, G.; Weck, G.; Mezouar, M.; Loubeyre, P. Hexagonal Layered Polymeric Nitrogen Phase Synthesized near 250 GPa. *Phys. Rev. Lett.* **2019**, *122*, 066001. [CrossRef]
43. Penumatcha, A.V.; Salazar, R.B.; Appenzeller, J. Analysing black phosphorus transistors using an analytic Schottky barrier MOSFET model. *Nat. Commun.* **2015**, *6*, 8948. [CrossRef]
44. Pizzi, G.; Gibertini, M.; Dib, E.; Marzari, N.; Iannaccone, G.; Fiori, G. Performance of arsenene and antimonene double-gate MOSFETs from first principles. *Nat. Commun.* **2016**, *7*, 12585. [CrossRef]
45. Ares, P.; Palacios, J.J.; Abellán, G.; Gómez-Herrero, J.; Zamora, F. Recent Progress on Antimonene: A New Bidimensional Material. *Adv. Mater.* **2018**, *30*, 1703771. [CrossRef] [PubMed]
46. Qiao, J.; Kong, X.; Hu, Z.X.; Yang, F.; Ji, W. High-mobility transport anisotropy and linear dichroism in few-layer black phosphorus. *Nat. Commun.* **2014**, *5*, 4475. [CrossRef]
47. Xia, F.; Wang, H.; Jia, Y. Rediscovering black phosphorus as an anisotropic layered material for optoelectronics and electronics. *Nat. Commun.* **2014**, *5*, 4458. [CrossRef]
48. Island, J.O.; Steele, G.A.; van der Zant, H.S.; Castellanos-Gomez, A. Environmental instability of few-layer black phosphorus. *2D Mater.* **2015**, *2*, 011002. [CrossRef]
49. Huang, Y.; Qiao, J.; He, K.; Bliznakov, S.; Sutter, E.; Chen, X.; Luo, D.; Meng, F.; Su, D.; Decker, J.; et al. Interaction of Black Phosphorus with Oxygen and Water. *Chem. Mater.* **2016**, *28*, 8330–8339. [CrossRef]
50. Tan, C.; Cao, X.; Wu, X.-J.; He, Q.; Yang, J.; Zhang, X.; Chen, J.; Zhao, W.; Han, S.; Nam, G.-H.; et al. Recent Advances in Ultrathin Two-Dimensional Nanomaterials. *Chem. Rev.* **2017**, *117*, 6225–6331. [CrossRef]
51. Lee, J.S.; Choi, S.H.; Yun, S.J.; Kim, Y.I.; Boandoh, S.; Park, J.-H.; Shin, B.G.; Ko, H.; Lee, S.H.; Kim, Y.-M.; et al. Wafer-scale single-crystal hexagonal boron nitride film via self-collimated grain formation. *Science* **2018**, *362*, 817–821. [CrossRef]
52. Wang, H.; Li, C.; Fang, P.; Zhang, Z.; Zhang, J.Z. Synthesis, properties, and optoelectronic applications of two-dimensional MoS_2 and MoS_2-based heterostructures. *Chem. Soc. Rev.* **2018**, *47*, 6101–6127. [CrossRef]
53. Hosseinzadeh, F.; Boochani, A.; Elahi, S.M.; Ghorannevis, Z. GdPtBi Heuslerene: Mechanical stability, half-metallic, magneto-optic, and thermoelectric properties by DFT. *Philos. Mag.* **2022**, *102*, 887–901. [CrossRef]
54. Bagheri, A.; Boochani, A.; Masharian, S.R. Huge Figure of Merit, Half-Metallic, and Optical Properties in n-Type CoVSb Heuslerene. *Int. J. Thermophys.* **2022**, *43*, 31. [CrossRef]
55. Blochl, P.E.; Jepsen, O.; Andersen, O.K. Improved tetrahedron method for Brillouin-zone integrations. *Phys. Rev. B.* **1994**, *49*, 16223. [CrossRef] [PubMed]
56. Boochani, A.; Jamal, M.; Shahrokhi, M.; Nowrozi, B.; Gholivand, M.B.; Khodadadi, J.; Sartipi, E.; Amiri, M.; Asshabi, M.; Yari, A. Ti_2VGe Heuslerene: Theoretical prediction of a novel 2D material. *J. Mater. Chem. C* **2019**, *7*, 13559–13572. [CrossRef]
57. Schwarz, K.; Blaha, P. Solid state calculations using WIEN2k. *Comput. Mater. Sci.* **2003**, *28*, 259–273. [CrossRef]
58. Boochani, A.; Nowrozi, B.; Khodadadi, J.; Solaymani, S.; Jalali-Asadabadi, S. Novel Graphene-like Co_2VAl (111): Case Study on Magnetoelectronic and Optical Properties by First-Principles Calculations. *J. Phys. Chem. C* **2017**, *121*, 3978–3986. [CrossRef]

59. Tran, F.; Blaha, P.; Schwarz, K.; Novák, P. Hybrid exchange-correlation energy functionals for strongly correlated electrons: Applications to transition-metal monoxides. *Phy. Rev. B* **2006**, *74*, 155108. [CrossRef]
60. Ofe, U.; Onuu, M.U.; Udoimuk, A.B. Electronic and structural properties of CaH_2 using GGA and GGA+ U approximation with WIEN 2K codes. *Int. J. Innov. Sci. Appl. Stud.* **2014**, *7*, 1071–1077.
61. Perdew, J.P. Generalized gradient approximation for solids and their surfaces. *Phys. Rev. Lett.* **2008**, *100*, 136406. [CrossRef]
62. Liechtenstein, A.I.; Anisimov, V.I.; Zaanen, J. Density-functional theory and strong interactions: Orbital ordering in Mott-Hubbard insulators. *Phys. Rev. B* **1995**, *52*, R5467–R5470. [CrossRef]
63. Jamal, M.; Bilal, M.; Ahmad, I.; Jalali-Asadabadi, S. IRelast package. *J. Alloys Compd.* **2018**, *735*, 569–579. [CrossRef]
64. Jamal, M.; Asadabadi, S.J.; Ahmad, I.; Aliabad, H.R. Elastic constants of cubic crystals. *Comput. Mater. Sci.* **2014**, *95*, 592–599. [CrossRef]
65. Giannozzi, P.; Baroni, S.; Bonini, N.; Calandra, M.; Car, R.; Cavazzoni, C.; Ceresoli, D.; Chiarotti, G.L.; Cococcioni, M.; Dabo, I. QUANTUM ESPRESSO: A modular and open-source software project for quantum simulations of materials. *J. Phys. Condens. Matter* **2009**, *21*, 395502. [CrossRef]
66. Giannozzi, P.; Andreussi, O.; Brumme, T.; Bunau, O.; Nardelli, M.B.; Calandra, M.; Car, R.; Cavazzoni, C.; Ceresoli, D.; Cococcioni, M.; et al. Advanced capabilities for materials modelling with QUANTUM ESPRESSO. *J. Phys. Condens. Matter* **2017**, *29*, 465901. [CrossRef] [PubMed]
67. Jamal, M.; Sarvestani, N.K.; Yazdani, A.; Reshak, A.H. Mechanical and thermodynamical properties of hexagonal compounds at optimized lattice parameters from two-dimensional search of the equation of state. *RSC Adv.* **2014**, *4*, 57903–57915. [CrossRef]
68. Shafiq, M.; Arif, S.; Ahmad, I.; Asadabadi, S.J.; Maqbool, M.; Aliabad, H.A.R. Elastic and mechanical properties of lanthanide monoxides. *J. Alloy. Compd.* **2015**, *618*, 292–298. [CrossRef]
69. Ahmad, S.; Ahmad, R.; Jalali-Asadabadi, S.; Ali, Z.; Ahma, I. First principle studies of structural, magnetic and elastic properties of orthorhombic rare-earth diaurides intermetallics RAu2 (R=La, Ce, Pr and Eu). *Mater. Chem. Phys.* **2018**, *212*, 44–50. [CrossRef]
70. IRelast2D Package Is Provided by M. Jamal. It Will Be as Part of the Commercial Code WIEN2K. Available online: http://www.wien2k.at/ (accessed on 12 February 2023).
71. Blaha, P.; Schwarz, K.; Tran, F.; Laskowski, R.; Madsen, G.K.H.; Marks, L.D. WIEN2k: An APW+ lo program for calculating the properties of solids. *J. Chem. Phys.* **2020**, *152*, 074101. [CrossRef]
72. Espinosa, H.D.; Bernal, R.A.; Filleter, T. In situ TEM electromechanical testing of nanowires and nanotubes. *Small* **2012**, *8*, 3233–3252. [CrossRef] [PubMed]
73. Yildirim, A.; Koc, H.; Deligoz, E. First-principles study of the structural, elastic, electronic, optical, and vibrational properties of intermetallic Pd_2Ga. *Chin. Phys. B* **2012**, *21*, 037101. [CrossRef]
74. Brik, M.G. First-principles calculations of electronic, optical and elastic properties of $ZnAl_2S_4$ and $ZnGa_2O_4$. *J. Phys. Chem. Solids* **2010**, *71*, 1435–1442. [CrossRef]
75. Chen, X.Q.; Niu, H.; Li, D.; Li, Y. Modeling hardness of polycrystalline materials and bulk metallic glasses. *Intermetallics* **2011**, *19*, 1275–1281. [CrossRef]
76. Tian, Y.; Xu, B.; Zhao, Z. Microscopic theory of hardness and design of novel superhard crystals. *Inte. J. Refract. Metal. Hard Mater.* **2012**, *33*, 93–106. [CrossRef]
77. Wu, S.; Fecher, G.H.; Naghavi, S.S.; Felser, C. Elastic properties and stability of Heusler compounds: Cubic Co_2YZ compounds with $L2_1$ structure. *J. Appl. Phys.* **2019**, *125*, 082523. [CrossRef]
78. Salehi, H.; Halvaei, M.; Amiri, P. Calculation of electronic, structural, optical and elastic properties of Heusler compounds (Co_2CrAl and Co_2CrGa). *J. R. Many-Body Syst.* **2018**, *8*, 69.
79. Blaha, P.; Schwarz, K.; Sorantin, P.; Trickey, S.B. Full-potential, linearized augmented plane wave programs for rystalline systems. *Comput. Phys. Commun.* **1990**, *59*, 399–415. [CrossRef]
80. Perdew, J.; Chevary, J.A.; Vosko, S.H.; Jackson, K.A.; Pederson, M.R.; Singh, D.J.; Fiolhais, C. Atoms, molecules, solids, and surfaces: Applications of the generalized gradient approximation for exchange and correlation. *Phys. Rev. B* **1992**, *46*, 6671–6687. [CrossRef]
81. Mouhat, F.; Coudert, F.X. Necessary and sufficient elastic stability conditions in various crystal systems. *Phys. Rev. B* **2014**, *90*, 224104. [CrossRef]
82. Zhang, S.H.; Zhang, R.F. AELAS: Automatic elastic property derivations via high-throughput first-principles computation. *Comput. Phys. Commun.* **2017**, *220*, 403–416. [CrossRef]
83. Chen, Y.; An, X.; Liao, X. Mechanical behaviors of nanowires. *Appl. Phys. Rev.* **2017**, *4*, 031104. [CrossRef]
84. Wu, B.; Heidelberg, A.; Boland, J.J. Mechanical properties of ultrahigh-strength gold nanowires. *Nat. Mater.* **2005**, *4*, 525–529. [CrossRef] [PubMed]
85. Herring, C.; Galt, J.K. Elastic and Plastic Properties of Very Small Metal Specimens. *Phys. Rev.* **1952**, *85*, 1060–1061. [CrossRef]
86. Brenner, S.S. Tensile Strength of Whiskers. *J. Appl. Phys.* **1956**, *27*, 1484–1491. [CrossRef]
87. Miller, R.E.; Shenoy, V.B. Size-dependent elastic properties of nanosized structural elements. *Nanotechnology* **2000**, *11*, 139–147. [CrossRef]
88. Zhu, T.; Li, J. Ultra-strength materials. *Prog. Mater. Sci.* **2010**, *55*, 710–757. [CrossRef]

89. Greer, J.R.; De Hosson, J.T.M. Plasticity in small-sized metallic systems: Intrinsic versus extrinsic size effect. *Prog. Mater. Sci.* **2011**, *56*, 654–724. [CrossRef]
90. Capelle, K.; Vignale, G.; Ullrich, C.A. Spin gaps and spin-flip energies in density-functional theory. *Phys. Rev. B* **2010**, *81*, 125114. [CrossRef]

Disclaimer/Publisher's Note: The statements, opinions and data contained in all publications are solely those of the individual author(s) and contributor(s) and not of MDPI and/or the editor(s). MDPI and/or the editor(s) disclaim responsibility for any injury to people or property resulting from any ideas, methods, instructions or products referred to in the content.